SIAM J. NUMER. ANAL.
Vol. 37, No. 1, pp. 105–130

SPATIAL FINITE DIFFERENCE APPROXIMATIONS FOR WAVE-TYPE EQUATIONS*

BENGT FORNBERG† AND MICHELLE GHRIST†

Abstract. The simplest finite difference approximations for spatial derivatives are centered, explicit, and applied to "regular" equispaced grids. Well-established generalizations include the use of implicit (compact) approximations and staggered grids. We find here that the combination of these two concepts, together with high formal order of accuracy, is very effective for approximating the first derivatives in space that occur in many wave-type PDEs.

Key words. finite differences, implicit approximation, compact approximation, staggered grid, pseudospectral method

AMS subject classifications. 65D25, 65N06, 65N35

PII. S0036142998335881

1. Introduction.

Wave equations, especially in two or more dimensions, are often formulated as first order systems. The primary requirements for numerical approximations of the first derivatives in space are

i. high accuracy,

ii. low operation count,

and the overall resulting method must also feature

iii. compatibility with curved interfaces and nonreflecting far field boundary conditions.

Several numerical approaches excel in one or sometimes two of these respects (e.g., finite elements and periodic pseudospectral (PS) methods). A combination of high-order interface techniques along material discontinuities and boundaries [3], [4] and an implicit staggered scheme for remaining areas of the computational domain meets all three requirements (near-spectral accuracy requiring only about four to five points per wavelength, about six to eight arithmetic operations for each spatial derivative at each grid point, with full spectral accuracy maintained at general interfaces). Figure 1 illustrates schematically how a composite method/grid for this approach can be structured in the case of the coupling of different media in a two-dimensional (2-D) calculation for Maxwell's equations.

This paper focuses on the problem of obtaining high accuracy economically on the "background" (x, y)-grid. At its (usually jagged) edges, this grid overlaps with a strip that follows the interface. Results on computations with this composite setup are reported in [4]. (In view of this intended usage, we do not discuss here the implementation of traditional boundary conditions.) Table 1 gives examples of the simplest first derivative approximations for each of the four stencil types considered here, explicit and implicit approximations on regular and staggered grids. The main topics of the remaining sections 2–9 are as follows:

2. illustrations of grid staggering,

*Received by the editors March 19, 1998; accepted for publication (in revised form) December 21, 1998; published electronically November 12, 1999.

http://www.siam.org/journals/sinum/37-1/33588.html

†Department of Applied Mathematics, University of Colorado, CB-526, Boulder, CO 80309 (fornberg@colorado.edu, michelle.ghrist@colorado.edu). The research of the first author was partially supported by NSF grant DMS-9706919 and by AFOSR/DARPA F49620-96-1-0426. The research of the second author was supported by NASA grant NPSC-OCG1035B and NSF grant DMS-9256335.

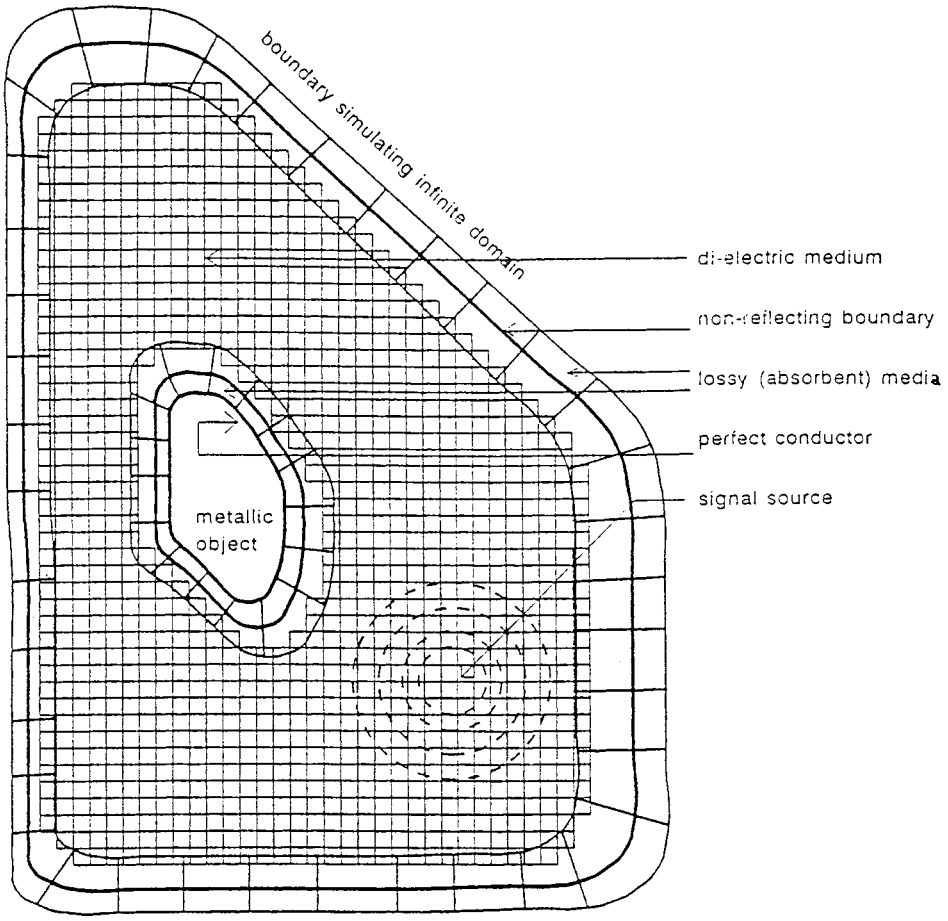

FIG. 1. *Schematic illustration of composite grid concept. In this case, we imagine solving Maxwell's equations in 2-D in a case where a metallic object (coated with an absorbing (lossy) medium) is illuminated with a radar source. Around the outer boundary is wrapped a strip-like domain which, along its middle, features a perfectly nonreflecting boundary between the main dielectric (e.g., vacuum) and a strong signal absorber. The grid densities (especially in the strips around the object and the boundary) would, in general, be considerably higher than shown. Implementation of strips with media interfaces is described in* [4]; *the methods in the present study apply to the Cartesian background grid.*

3. simple symbolic algebra code that will calculate the weights for all stencils of the kinds described,

4. tables of weights and formulas for weights in the limit of increasing orders of accuracy,

5. observation that in the limit of increasing orders, the implicit and the explicit formulas become equivalent in terms of how derivative value depends on function values,

6. comparisons of operation counts,

7. comparisons of accuracies and cost-effectiveness,

8. test example, and

9. summary of our observations.

TABLE 1
Examples of finite difference approximations.

Grid type	Approximation type	Lowest order stencil of given type		Leading error term	Parameters for weights code (in section 3) m	s	d	n
Regular	Explicit	$f'(x)$	$= [-\frac{1}{2}f(x-h) + \frac{1}{2}f(x+h)]/h$	$\frac{1}{6}h^2 f^{(3)}(x)$	1	1	0	2
	Implicit	$\frac{1}{6}f'(x-h) + \frac{2}{3}f'(x) + \frac{1}{6}f'(x+h)$	$= [-\frac{1}{2}f(x-h) + \frac{1}{2}f(x+h)]/h$	$-\frac{1}{180}h^4 f^{(5)}(x)$	1	0	2	2
Staggered	Explicit	$f'(x)$	$= [-f(x-\frac{h}{2}) + f(x+\frac{h}{2})]/h$	$\frac{1}{24}h^2 f^{(3)}(x)$	1	$\frac{1}{2}$	0	1
	Implicit	$\frac{1}{24}f'(x-h) + \frac{11}{12}f'(x) + \frac{1}{24}f'(x+h)$	$= [-f(x-\frac{h}{2}) + f(x+\frac{h}{2})]/h$	$-\frac{17}{5760}h^4 f^{(5)}(x)$	1	$-\frac{1}{2}$	2	1

On most issues that are covered, additional information (e.g., derivations of most formulas quoted here) can be found in [9].

2. Illustrations of grid staggering. It is fortunate that most linear wave equations of general interest—in any number of space dimensions—have only a few of all possible spatial derivatives present and that these tend to appear in such a way that grid staggering becomes straightforward. (This is most likely related to how the equations arise from conservation laws; however, we are unaware of any clear references supporting this.) Figures 2(a)–(c) illustrate staggering in three representative cases: one-dimensional (1-D) acoustic, 2-D elastic, and three-dimensional (3-D) Maxwell's equations. In each case, we contrast two layouts of spatial grids, regular vs. staggered, both featuring the same density of grid data. The ease of creating staggered layouts for all major linear wave equations makes the present analysis widely applicable.

One can also stagger in time, as is done (using leap-frog), e.g., in the Yee scheme for time-domain computational electrodynamics [16], [20], [22]. A follow-up study to this one [10] discusses higher order time staggering.

3. Algorithm for FD weights. The weights in any of the stencils we discuss in this paper can be calculated by the two-line Mathematica algorithm,

```
t=Pade[x^s*Log[x]^m,{x,1,n,d}];
{CoefficientList[Denominator[t],x],CoefficientList[Numerator[t],x]/h^m}
```

or in Maple,

```
t:=pade (x^s*ln(x)^m,x=1,[n,d]):
coeff (expand (denom(t)),x,i)        $i=0..d;
coeff (expand (numer(t)),x,i)/h^m     $i=0..n;
```

In both cases, a Padé package must first be loaded; this is done with the commands `<<Calculus‘Pade‘` or `with (numapprox):`, respectively. In these lines of code, `m` denotes what order derivative we want to approximate. (This will be one in all cases considered in this paper but may be any nonnegative integer; the case `m=0` will generate interpolation formulas.) The remaining three input parameters `s`, `d`, and `n` describe the shape of the stencil, as illustrated in Figure 3. The parameter `s` may be any real number (of either sign); `d` and `n` must be nonnegative integers.

For the first derivative (i.e., `m=1`) and with the stencil shown in Figure 3, the Mathematica output becomes

$$\left\{\left\{\frac{9}{80},\frac{31}{40},\frac{9}{80}\right\},\left\{-\frac{17}{240h},-\frac{63}{80h},\frac{63}{80h},\frac{17}{240h},\right\}\right\} \tag{1}$$

(cf. the case $n = 2$ in Table 6). We conclude this section by explaining why the Padé algorithm works in the special case above (following the argument in [8], this generalizes immediately to other values of `m`, `s`, `d`, and `n`).

We search for coefficients b_i and c_i so that

$$\begin{aligned} b_0 f'(x-h) + b_1 f'(x) + b_2 f'(x+h) \approx{}& c_0 f\left(x-\frac{3}{2}h\right) + c_1 f\left(x-\frac{1}{2}h\right) \\ &+ c_2 f\left(x+\frac{1}{2}h\right) + c_3 f\left(x+\frac{3}{2}h\right) \end{aligned} \tag{2}$$

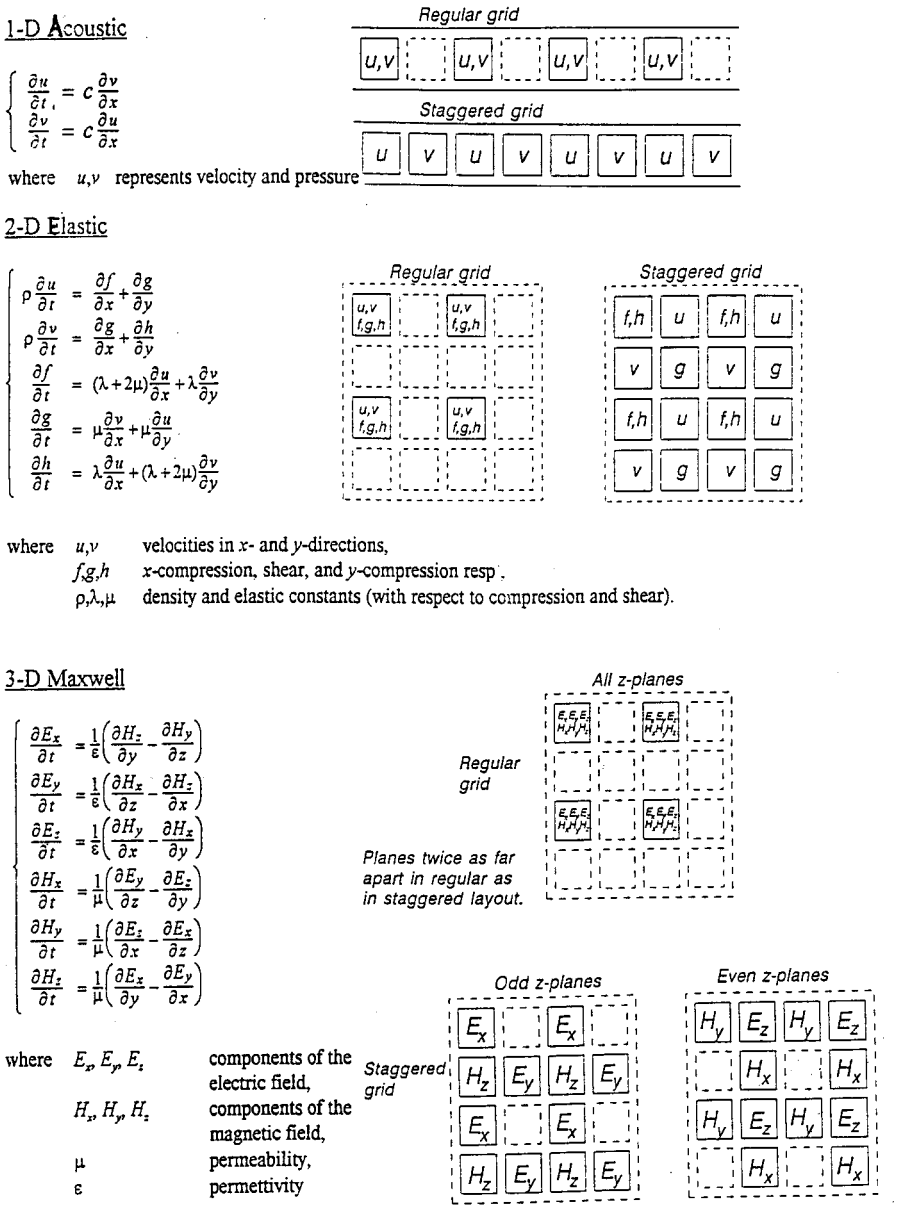

FIG. 2. *Illustrations of staggering for some linear wave equations.*

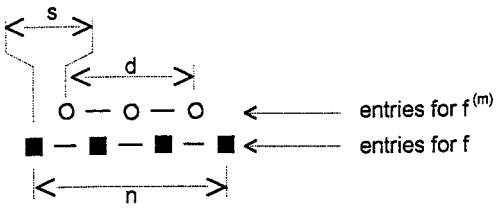

FIG. 3. *Schematic illustration of the notation used in the Padé weight algorithm in a staggered case; here* $s = \frac{1}{2}$, $d = 2$, *and* $n = 3$. *(All distances s, d, n are in units of the step length h.) The notation in this and subsequent illustrations of stencils follows the convention (as adopted, e.g., in* [7]):

○/● *derivative entry,*
□/■ *function entry.*

The symbols are unfilled or filled, depending on whether the corresponding derivative or function value would be unknown (i.e., to be solved for) or known in the anticipated application of the stencil.

becomes exact for polynomials $f(x)$ of as high degree as possible. Substituting $f(x) = e^{i\omega x}$ into (2) gives

$$i\omega[b_0 e^{-i\omega h} + b_1 + b_2 e^{i\omega h}]e^{i\omega x} \approx [c_0 e^{-i\omega\frac{3}{2}h} + c_1 e^{-i\omega\frac{1}{2}h} + c_2 e^{i\omega\frac{1}{2}h} + c_3 e^{i\omega\frac{3}{2}h}]e^{i\omega x}$$

with the new goal being to make the relation as accurate as possible if locally expanded around $\omega = 0$ (cf. [21, pp. 24–26]). After canceling out the factor $e^{i\omega x}$ and substituting $e^{i\omega h} = \xi$ (i.e., $i\omega h = \ln\xi$), we get

$$\xi^{\frac{1}{2}}\frac{\ln\xi}{h} \approx \frac{c_0 + c_1\xi + c_2\xi^2 + c_3\xi^3}{b_0 + b_1\xi + b_2\xi^2}. \tag{3}$$

This needs to be as accurate as possible around $\xi = 1$. Padé expansions of the left-hand side (LHS) around $\xi = 1$ to order [3, 2] produces the desired coefficients:

$$\xi^{\frac{1}{2}}\frac{\ln\xi}{h} \approx \frac{1}{h}\frac{(x-1) + (x-1)^2 + \frac{17}{240}(x-1)^3}{1 + (x-1) + \frac{9}{80}(x-1)^2} = \frac{\left(-\frac{17}{240} - \frac{63}{80}x + \frac{63}{80}x^2 + \frac{17}{240}x^3\right)\frac{1}{h}}{\left(\frac{9}{80} + \frac{31}{40}x + \frac{9}{80}x^2\right)}.$$

The notation above in the description of the weights algorithm was chosen to agree with [8]. It is noted there that the explicit case (d = 0) can be handled even more easily by substituting a Taylor expansion for the Padé expansion used here (since the denominator in (3) is then one). Hereafter in this paper, we consider only first derivative approximations, and we use m, n, and k to denote stencil entries as illustrated in Figure 4.

4. Tables for some weights and formulas for limits of infinite order. Tables 2–7 provide numerical values for the weights in the cases that are of main interest. Closed-form expressions for the entries in all these tables (in terms of n and k) are given in [9]. From these follow the quoted limits for k fixed and $n \to \infty$. Table 8 gives a more general integral formulation of these limits and shows that these integrals can be evaluated explicitly.

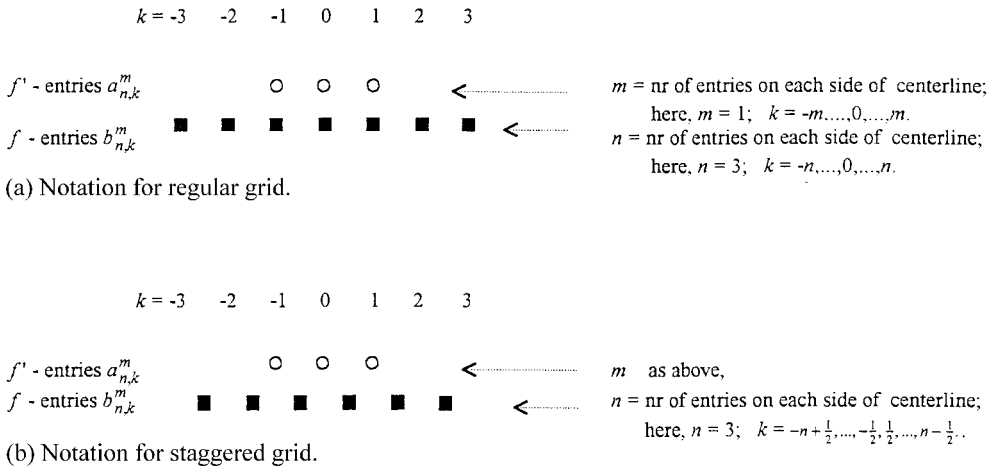

FIG. 4. *Notation used to index entries in regular and staggered stencils.*

The following is a very brief heuristic argument that leads to the limit expressions in Table 8. Again, one case suffices to illustrate the general argument. We consider the following tridiagonal (3-diagonal) regular grid case:

(4)

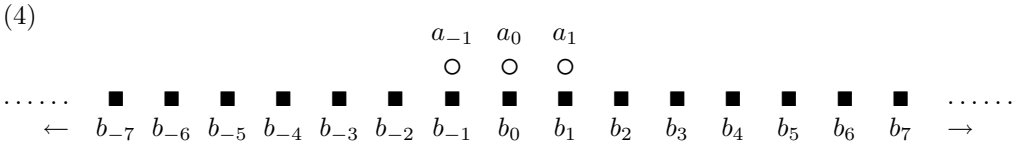

As their widths increase, the finite-sized stencils are exact for polynomials of increasingly high orders. The infinite-width limit stencil will also then be exact for all trigonometric modes $\sin \omega x$ (for which the derivative is $\omega \cos \omega x$). When applied at $x = 0$ and with step size $h = 1$, this gives

(5)

$$\omega(a_{-1}\cos(-\omega) + a_0 \cos(0\omega) + a_1 \cos(\omega)) = 2(b_1 \sin\omega + b_2 \sin 2\omega + b_3 \sin 3\omega + \cdots)$$

(holding for all ω). We next make the very reasonable assumptions that

i. the desired limit represents the most accurate derivative approximation available of the form (4), and

ii. the derivative, being a local property of a function, is best approximated when the coefficients b_k decay to zero as fast as possible (subject to (5) holding true).

The LHS of (5) is a product of the step function ω (which jumps at $\omega = \pm\pi$ when periodically extended) and a periodic function $a_0 + 2a_1 \cos\omega$ (since by symmetry $a_{-1} = a_1$). The decay rate of the Fourier coefficients of this product is maximal if the LHS is as smooth as possible at $\omega = \pm\pi$, i.e., when $a_0 + 2a_1 \cos\omega$ has a zero there of as high degree as possible. This occurs for $a_0 = \frac{1}{2}$, $a_1 = \frac{1}{4}$, and $a_0 + 2a_1 \cos\omega = (\cos\frac{\omega}{2})^2$. We can thus (in the tridiagonal ($m = 1$)-case) obtain the coefficients as

$$a_k = \frac{1}{\pi}\int_0^\pi \cos\omega k \left(\cos\frac{\omega}{2}\right)^2 d\omega \text{ and}$$
$$b_k = \frac{1}{\pi}\int_0^\pi \omega \sin\omega k \left(\cos\frac{\omega}{2}\right)^2 d\omega.$$

The case of general m follows completely analogously.

TABLE 2
Weights for explicit, regular grid FD formulas.

	Accuracy		Weights $b^0_{n,k}$ for f										
$n=$	order	$k=$	-5	-4	-3	-2	-1	0	1	2	3	4	5
1	2						$-\frac{1}{2}$	0	$\frac{1}{2}$				
2	4					$\frac{1}{12}$	$-\frac{2}{3}$	0	$\frac{2}{3}$	$-\frac{1}{12}$			
3	6				$-\frac{1}{60}$	$\frac{3}{20}$	$-\frac{3}{4}$	0	$\frac{3}{4}$	$-\frac{3}{20}$	$\frac{1}{60}$		
4	8			$\frac{1}{280}$	$-\frac{4}{105}$	$\frac{1}{5}$	$-\frac{4}{5}$	0	$\frac{4}{5}$	$-\frac{1}{5}$	$\frac{4}{105}$	$-\frac{1}{280}$	
5	10		$-\frac{1}{1260}$	$\frac{5}{504}$	$-\frac{5}{84}$	$\frac{5}{21}$	$-\frac{5}{6}$	0	$\frac{5}{6}$	$-\frac{5}{21}$	$\frac{5}{84}$	$-\frac{5}{504}$	$\frac{1}{1260}$
...	...		...	...	...	...	...	...	...	...	...	...	...
Limit as $n \to \infty$:													
			$a^0_{n,0} = 1$ for all n;				$b^0_{\infty,k} = \begin{cases} 0 & k = 0 \\ \frac{(-1)^{k+1}}{k} & k \neq 0 \end{cases}$					

TABLE 3
Weights for implicit 3-diagonal, regular grid FD formulas.

	Accuracy		Weights $a^1_{n,k}$ for f'							Weights $b^1_{n,k}$ for f						
$n=$	order	$k=$	-1	0	1	-5	-4	-3	-2	-1	0	1	2	3	4	5
1	4		$\frac{1}{6}$	$\frac{2}{3}$	$\frac{1}{6}$					$-\frac{1}{2}$	0	$\frac{1}{2}$				
2	6		$\frac{1}{5}$	$\frac{3}{5}$	$\frac{1}{5}$				$-\frac{1}{60}$	$-\frac{7}{15}$	0	$\frac{7}{15}$	$\frac{1}{60}$			
3	8		$\frac{3}{14}$	$\frac{4}{7}$	$\frac{3}{14}$			$\frac{1}{840}$	$-\frac{1}{35}$	$-\frac{25}{56}$	0	$\frac{25}{56}$	$\frac{1}{35}$	$-\frac{1}{840}$		
4	10		$\frac{2}{9}$	$\frac{5}{9}$	$\frac{2}{9}$		$-\frac{1}{7560}$	$\frac{1}{378}$	$-\frac{1}{27}$	$-\frac{13}{30}$	0	$\frac{13}{30}$	$\frac{1}{27}$	$-\frac{1}{378}$	$\frac{1}{7560}$	
5	12		$\frac{5}{22}$	$\frac{6}{11}$	$\frac{5}{22}$	$\frac{1}{55440}$	$-\frac{1}{2772}$	$\frac{5}{1232}$	$-\frac{10}{231}$	$-\frac{14}{33}$	0	$\frac{14}{33}$	$\frac{10}{231}$	$-\frac{5}{1232}$	$\frac{1}{2772}$	$-\frac{1}{55440}$
...	...		...	...	...	...	...	...	...	...	...	...	...	...	...	...

Limit as $n \to \infty$:

$$a^1_{\infty,k} = \begin{cases} \frac{1}{2} & k = 0 \\ \frac{1}{4} & k = \pm 1 \end{cases} ; \qquad b^1_{\infty,k} = \begin{cases} 0 & k = 0 \\ \frac{3}{8}\text{sign}(k) & k = \pm 1 \\ \frac{1}{2}\frac{(-1)^k}{(k-1)(k)(k+1)} & |k| \geq 2 \end{cases}$$

TABLE 4
Weights for implicit 5-diagonal, regular grid FD formulas.

	Accuracy		Weights $a^2_{n,k}$ for f'					Weights $b^2_{n,k}$ for f										
n	order	$k=$	-2	-1	0	1	2	-5	-4	-3	-2	-1	0	1	2	3	4	5
1	6		$-\frac{1}{180}$	$\frac{17}{90}$	$\frac{19}{30}$	$\frac{17}{90}$	$-\frac{1}{180}$					$-\frac{1}{2}$	0	$\frac{1}{2}$				
2	8		$\frac{1}{70}$	$\frac{8}{35}$	$\frac{18}{35}$	$\frac{8}{35}$	$\frac{1}{70}$				$-\frac{5}{84}$	$-\frac{8}{21}$	0	$\frac{8}{21}$	$\frac{5}{84}$			
3	10		$\frac{1}{42}$	$\frac{5}{21}$	$\frac{10}{21}$	$\frac{5}{21}$	$\frac{1}{42}$			$-\frac{1}{1260}$	$-\frac{101}{1260}$	$-\frac{85}{252}$	0	$\frac{85}{252}$	$\frac{101}{1260}$	$\frac{1}{1260}$		
4	12		$\frac{1}{33}$	$\frac{8}{33}$	$\frac{5}{11}$	$\frac{8}{33}$	$\frac{1}{33}$		$\frac{1}{27720}$	$-\frac{2}{1155}$	$-\frac{91}{990}$	$-\frac{14}{45}$	0	$\frac{14}{45}$	$\frac{91}{990}$	$\frac{2}{1155}$	$-\frac{1}{27720}$	
5	14		$\frac{5}{143}$	$\frac{35}{143}$	$\frac{63}{143}$	$\frac{35}{143}$	$\frac{5}{143}$	$-\frac{1}{360360}$	$\frac{1}{10296}$	$-\frac{3}{1144}$	$-\frac{199}{2002}$	$-\frac{42}{143}$	0	$\frac{42}{143}$	$\frac{199}{2002}$	$\frac{3}{1144}$	$-\frac{1}{10296}$	$\frac{1}{360360}$
...	...		...	...	...	...	...	...	...	...	...	...	...	...	...	...	...	...

Limit as $n \to \infty$:

$$a^2_{\infty,k} = \begin{cases} \frac{3}{8} & k = 0 \\ \frac{1}{4} & k = \pm 1 \\ \frac{1}{16} & k = \pm 2 \end{cases} \quad ; \qquad b^2_{\infty,k} = \begin{cases} 0 & k = 0 \\ \frac{5}{24}\text{sign}(k) & k = \pm 1 \\ \frac{25}{192}\text{sign}(k) & k = \pm 2 \\ \frac{3}{2}\frac{(-1)^{k+1}}{(k-2)(k-1)(k)(k+1)(k+2)} & |k| > 2 \end{cases}$$

TABLE 5
Weights for explicit, staggered grid FD formulas.

	Accuracy		Weights $b^0_{n,k}$ for f											
$n=$	order	$k=$	$-11/2$	$-9/2$	$-7/2$	$-5/2$	$-3/2$	$-1/2$	$1/2$	$3/2$	$5/2$	$7/2$	$9/2$	$11/2$
1	2							-1	1					
2	4						$\frac{1}{24}$	$-\frac{9}{8}$	$\frac{9}{8}$	$-\frac{1}{24}$				
3	6					$-\frac{3}{640}$	$\frac{25}{384}$	$-\frac{75}{64}$	$\frac{75}{64}$	$-\frac{25}{384}$	$\frac{3}{640}$			
4	8				$\frac{5}{7168}$	$-\frac{49}{5120}$	$\frac{245}{3072}$	$-\frac{1225}{1024}$	$\frac{1224}{1024}$	$-\frac{245}{3072}$	$\frac{49}{5120}$	$-\frac{5}{7168}$		
5	10			$-\frac{35}{294912}$	$\frac{405}{229376}$	$-\frac{567}{40960}$	$\frac{735}{8192}$	$-\frac{19845}{16384}$	$\frac{19845}{16384}$	$-\frac{735}{8192}$	$\frac{567}{40960}$	$-\frac{405}{229376}$	$\frac{35}{294912}$	
6	12		$\frac{63}{2883584}$	$-\frac{847}{2359296}$	$\frac{5445}{1835008}$	$-\frac{22869}{1310720}$	$\frac{12705}{131072}$	$-\frac{160083}{131072}$	$\frac{160083}{131072}$	$-\frac{12705}{13107}$	$\frac{22869}{1310720}$	$-\frac{5445}{1835008}$	$\frac{847}{2359296}$	$-\frac{63}{2883584}$
...	...		...	...	...	...	...	...	...	...	...	...	...	...
Limit as $n \to \infty$:														
			$a^0_{n,0} = 1$ for all n;					$b^0_{\infty,k} = \frac{(-1)^{k-1/2}}{\pi k^2}$						

TABLE 6
Weights for implicit 3-diagonal, staggered grid FD formulas.

	Accuracy		Weights $a^1_{n,k}$ for f'			Weights $b^1_{n,k}$ for f									
n	order	$k=$	-1	0	1	$-9/2$	$-7/2$	$-5/2$	$-3/2$	$-1/2$	$1/2$	$3/2$	$5/2$	$7/2$	$9/2$
1	4		$\frac{1}{24}$	$\frac{11}{12}$	$\frac{1}{24}$					-1	1				
2	6		$\frac{9}{80}$	$\frac{31}{40}$	$\frac{9}{80}$				$-\frac{17}{240}$	$-\frac{63}{80}$	$\frac{63}{80}$	$\frac{17}{240}$			
3	8		$\frac{25}{168}$	$\frac{59}{84}$	$\frac{25}{168}$			$\frac{61}{40320}$	$-\frac{925}{8064}$	$-\frac{2675}{4032}$	$\frac{2675}{4032}$	$\frac{925}{8064}$	$-\frac{61}{40320}$		
4	10		$\frac{49}{288}$	$\frac{95}{144}$	$\frac{49}{288}$		$-\frac{43}{430080}$	$\frac{343}{110592}$	$-\frac{78841}{552960}$	$-\frac{64925}{110592}$	$\frac{64925}{110592}$	$\frac{78841}{552960}$	$-\frac{343}{110592}$	$\frac{43}{430080}$	
5	12		$\frac{81}{440}$	$\frac{139}{220}$	$\frac{81}{440}$	$\frac{221}{22708224}$	$-\frac{15957}{63078400}$	$\frac{70821}{15769600}$	$-\frac{364119}{2252800}$	$-\frac{96579}{180224}$	$\frac{96579}{180224}$	$\frac{364119}{2252800}$	$-\frac{70821}{15769600}$	$\frac{15957}{63078400}$	$-\frac{221}{22708224}$
...	...		...	...	...	...	...	...	...	...	...	...	...	...	...

Limit as $n \to \infty$:

$$a^1_{\infty,k} = \begin{cases} \frac{1}{2} & k = 0 \\ \frac{1}{4} & k = \pm 1 \end{cases} \quad ; \qquad b^1_{\infty,k} = \frac{(-1)^{k+\frac{1}{2}}}{2\pi} \frac{3k^2-1}{[(k-1)k(k+1)]^2}$$

TABLE 7
Weights for implicit 5-diagonal, staggered grid FD formulas.

			Weights $a^2_{n,k}$ for f'							Weights $b^2_{n,k}$ for f						
n	Accuracy order	$k=$	-2	-1	0	1	2	$-7/2$	$-5/2$	$-3/2$	$-1/2$	$1/2$	$3/2$	$5/2$	$7/2$
1	6		$-\frac{17}{5760}$	$\frac{77}{1440}$	$\frac{863}{960}$	$\frac{77}{1440}$	$-\frac{17}{5760}$				-1	1			
2	8		$\frac{183}{76160}$	$\frac{3057}{19040}$	$\frac{3667}{5440}$	$\frac{3057}{19040}$	$\frac{183}{76160}$			$-\frac{367}{2856}$	$-\frac{585}{952}$	$\frac{585}{952}$	$\frac{367}{2856}$		
3	10		$\frac{1075}{109312}$	$\frac{48425}{245952}$	$\frac{288529}{491904}$	$\frac{48425}{245952}$	$\frac{1075}{109312}$		$-\frac{69049}{14757120}$	$-\frac{505175}{2951424}$	$-\frac{683425}{1475712}$	$\frac{683425}{1475712}$	$\frac{505175}{2951424}$	$\frac{69049}{14757120}$	
4	12		$\frac{54145}{3269376}$	$\frac{879403}{4086720}$	$\frac{1461701}{2724480}$	$\frac{879403}{4086720}$	$\frac{54145}{3269376}$	$\frac{939109}{13731379200}$	$-\frac{19618669}{1961625600}$	$-\frac{124703971}{653875200}$	$-\frac{2698675}{7133184}$	$\frac{2698675}{7133184}$	$\frac{124703971}{653875200}$	$\frac{19618669}{1961625600}$	$-\frac{939109}{13731379200}$
...	...		...	...	...	...	...	...	...	...	...	...	...	...	...

Limit as $n \to \infty$:

$$a^2_{\infty,k} = \begin{cases} \frac{3}{8} & k = 0 \\ \frac{1}{4} & k = \pm 1 \\ \frac{1}{16} & k = \pm 2 \end{cases} ; \qquad b^2_{\infty,k} = \frac{(-1)^{k-\frac{1}{2}}}{2\pi} \frac{3(4-15k^2+5k^4)}{[(k-2)(k-1)k(k+1)(k+2)]^2}$$

TABLE 8
Limits of weights as $n \to \infty$ for schemes with $2m+1$ diagonals, $m = 0, 1, 2, \ldots$.

Limit	Integral form	Explicit form
Regular grid (k integer)		
$a^m_{\infty,k} =$	$\frac{1}{\pi}\int_0^\pi \cos(kx)\left(\cos\left(\frac{x}{2}\right)\right)^{2m} dx =$	$\begin{cases} \frac{1}{2^{2m}}\frac{(2m)!}{(m-k)!(m+k)!} & \lvert k\rvert \le m \\ 0 & \lvert k\rvert > m \end{cases}$
$b^m_{\infty,k} =$	$\frac{1}{\pi}\int_0^\pi x\sin(kx)\left(\cos\left(\frac{x}{2}\right)\right)^{2m} dx =$	$\begin{cases} 0 & k = 0 \\ \frac{(\mathrm{sign}k)(2m)!\sum_{j=1-\lvert k\rvert}^{\lvert k\rvert} 1/(j+m)}{2^{2m}(m-k)!(m+k)!} & 0 < \lvert k\rvert \le m \\ \frac{(-1)^{k+m+1}(2m)!}{2^{2m}\prod_{j=-m}^{m}(k+j)} & \lvert k\rvert > m \end{cases}$

Staggered grid, same as above except as follows:

- For the $b^m_{\infty,k}$-coefficients, k is not an integer but a "half-integer."
- In the $b^m_{\infty,k}$-explicit form, the formula above for $0 < |k| \le m$ applies in all cases. The sum runs over half-integers, and $(m-k)!(m+k)!$ needs to be interpreted as $\Gamma(m-k+1)\Gamma(m+k+1)$.

The literature on both regular and staggered explicit finite difference schemes is very extensive. (This also includes some schemes that have been designed with the goal of enhancing the accuracy for certain frequencies rather than maximizing formal order of accuracy [13], [14], [18].) Implicit regular schemes have been derived and studied on numerous occasions, e.g., [1], [2], [11], [12], [17], and [19]. Kopal [15] presents tables which allow easy calculation of weights in numerous schemes, including cases that combine staggering with implicitness (compactness). However, we are not aware of any references which test and analyze such combined schemes.

5. Equivalence between implicit and explicit formulas. An explicit FD stencil directly expresses how the approximation of a derivative is influenced by changes of function values at different locations. For regular grids—as the order of accuracy increases (i.e., $n \to \infty$)—the weights approach $b^0_{\infty,k} = \frac{(-1)^{k+1}}{k}$ ($k \neq 0$; cf. Table 2, [5], and [7, pp. 20–22]). The derivative approximation depends significantly on function values quite far away (in contrast with the exact derivative being a strictly local property of a function). For the tridiagonal implicit stencil, the decay of the weights is much faster: $b^1_{\infty,k} = \frac{1}{2}\frac{(-1)^k}{(k-1)k(k+1)}$ ($|k| \geq 2$; cf. Table 3). Superficially, it might appear that these approximations remain more "local." However, to actually obtain derivative approximations, we need to solve a tridiagonal system. The *equivalent explicit scheme* (obtained through multiplying with the inverse of this infinite tridiagonal matrix) will turn out to be equally globally coupled as the original explicit scheme. The same will hold true if we have five or more diagonals; in the limit of increasing order, these schemes all become identical.

In the staggered case, all implicit schemes similarly have the equivalent explicit scheme limit of $b_{\infty,k} = \frac{(-1)^{k-1/2}}{\pi k^2}$. In all cases—regular and staggered grids and of any order—equivalent explicit schemes can be found as illustrated in (6):

(6)

$$\begin{bmatrix} \ddots & \ddots & \ddots & & & & & & & & \\ \ddots & \ddots & \ddots & \ddots & & & & & & & \\ \ddots & \ddots & \ddots & \ddots & \ddots & & & & & & \\ & \ddots & \ddots & \ddots & \ddots & \ddots & & & & & \\ & & a^m_{n,-m} & \cdots & a^m_{n,0} & \cdots & a^m_{n,m} & & & & \\ & & & \ddots & \ddots & \ddots & \ddots & \ddots & & & \\ & & & & \ddots & \ddots & \ddots & \ddots & \ddots & & \\ & & & & & \ddots & \ddots & \ddots & \ddots & \ddots & \\ & & & & & & \ddots & \ddots & \ddots & \ddots & \\ & & & & & & & \ddots & \ddots & \ddots & \end{bmatrix}^{-1} \begin{bmatrix} \vdots \\ \vdots \\ \vdots \\ 0 \\ \times \\ \times \\ \times \\ \times \\ \times \\ \times \\ 0 \\ \vdots \\ \vdots \end{bmatrix} = \begin{bmatrix} \vdots \\ \vdots \\ \vdots \\ \times \\ \times \\ \times \\ \times \\ \times \\ \times \\ \times \\ \vdots \\ \vdots \end{bmatrix}.$$

Symmetric banded Toeplitz matrix; Weights $b_{n,k}$; Equivalent explicit weights

The inverse of the matrix can be written down in closed form (as follows from a consideration of the Fourier convolution theorem); it is again symmetric and Toeplitz

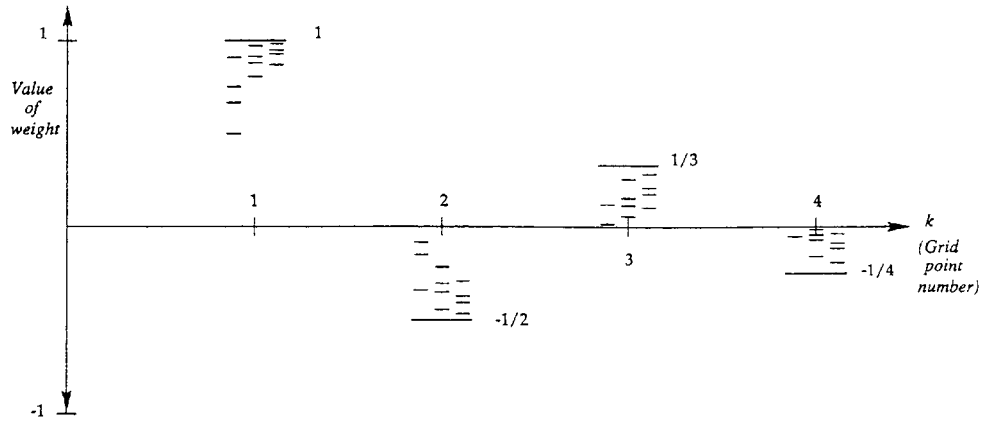

FIG. 5(a). *Equivalent weights for regular grid case. For the legend, see Figure* 5(c). *Note that in the explicit case, the weights are* 0 *for* $n < k$.

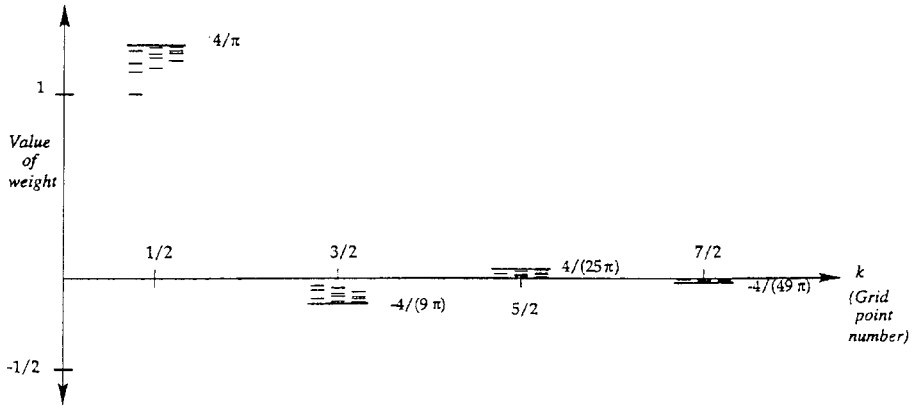

FIG. 5(b). *Equivalent weights for staggered grid case. For the legend, see Figure* 5(c). *Note that in the explicit case, the weights are* 0 *for* $n < k$.

with the entries along diagonal k

$$d_k = \frac{1}{2\pi} \int_{-\pi}^{\pi} \frac{\cos kx}{a_{n,0}^m + 2\sum_{j=1}^m a_{n,j}^m \cos jx}\, dx. \tag{7}$$

For example, in the regular grid tridiagonal case ($m = 1$) we have

$$a_{n,k}^1 = \begin{cases} \dfrac{n+1}{2n+1}, & k = 0, \\ \dfrac{n}{2(2n+1)}, & k = \pm 1, \end{cases}$$

and (7) then gives

$$d_k = \sqrt{2n+1} \cdot \left\{ -1 + \frac{1}{n}(\sqrt{2n+1} - 1) \right\}^{|k|}.$$

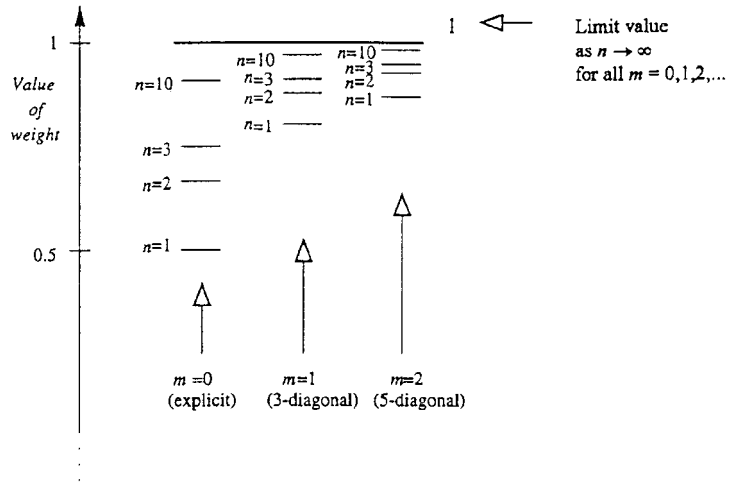

FIG. 5(c). *Detailed legend for Figures* 5(a) *and* 5(b), *as illustrated by the* $(k = 1)$*-case of Figure* 5(a).

Figure 5 graphically illustrates how the equivalent weights compare for the different schemes. From the point of locality, we find little advantage in using implicit schemes. Grid staggering is seen as more important in this respect.

The limits as $n \to \infty$ for both regular and staggered grids, if implemented on periodic data, become identical to the respective periodic PS methods [6], [7].

6. Comparison between operation counts. Regarding the number of arithmetic operations required to obtain the derivative at a grid point, we can note the following:

- There is no need to make any distinction between regular and staggered grids; their operation counts are identical (when expressed in n and number of diagonals).
- In the implicit cases, the LU factorization can be prestored. The entries in these matrices do not depend on the system size; i.e., one copy suffices even if the domain geometry is such that we have to solve systems of different sizes.
- One example of an operation count suffices to illustrate the general counting process. Consider the 3-diagonal regular grid $(n = 1)$-case with weights

$$\left[\frac{1}{6}\ \frac{2}{3}\ \frac{1}{6}\right] f' = \left[-\frac{1}{2}\ 0\ \frac{1}{2}\right] f.$$

TABLE 9

Operation count to calculate f' *at one grid point when using the different schemes. (There is no difference here between regular and staggered grids.)*

	$n=1$	2	3	4	$\cdots$	General n
Explicit	2	5	8	11	$\cdots$	$3n-1$
3-diag.	6	9	12	15	$\cdots$	$3n+3$
5-diag.	10	13	16	19	$\cdots$	$3n+7$
$\cdots$	$\cdots$	$\cdots$	$\cdots$	$\cdots$	$\cdots$	$\cdots$
k-diag.	$2k$	$2k+3$	$2k+6$	$2k+9$	$\cdots$	$2k+3n-3$

TABLE 10
Leading error terms for different first derivative approximations.

	Accuracy order	$p =$	2	4	6	8	10	p	Relationship between p and n; $p =$
	Type of error term		$h^2 f^{(3)}(x)$	$h^4 f^{(5)}(x)$	$h^6 f^{(7)}(x)$	$h^8 f^{(9)}(x)$	$h^{10} f^{(11)}(x)$	$h^p f^{(p+1)}(x)$	
Coefficients for leading error terms	*Regular grid*								
	Explicit		$\frac{1}{6}$	$-\frac{1}{30}$	$\frac{1}{140}$	$-\frac{1}{630}$	$\frac{1}{2772}$	$\frac{(-1)^{n+1}(n!)^2}{(2n+1)!}$	$2n$
	3-diag.		-	$-\frac{1}{180}$	$\frac{1}{2100}$	$-\frac{1}{17640}$	$\frac{1}{124740}$	$\frac{(-1)^n (n!)^2 (n+1)}{(2n+3)\ (2n+1)}$	$2n+2$
	5-diag.		-	-	$\frac{1}{1512}$	$-\frac{1}{44100}$	$\frac{1}{582120}$	$\frac{(-1)^{n+1} 6 (n!)^2 (n+1)(n+2)}{(2n+5)!(2n+1)(2n+3)}$	$2n+4$
	Staggered grid								
	Explicit		$\frac{1}{24}$	$-\frac{3}{640}$	$\frac{5}{7168}$	$-\frac{35}{294912}$	$\frac{63}{2883584}$	$\frac{(-1)^{n+1}(2n)!}{2^{4n}(n!)^2(2n+1)}$	$2n$
	3-diag.		-	$-\frac{17}{5760}$	$\frac{61}{358400}$	$-\frac{215}{14450688}$	$\frac{1547}{934281216}$	$\frac{(-1)^n (2n-1)!(12n^2+8n-3)}{2^{4n+2}(n!)(n+1)!(2n+1)^2(2n+3)}$	$2n+2$
	5-diag.		-	-	$\frac{367}{967680}$	$-\frac{69049}{6141542400}$	$\frac{939109}{1396283277312}$	$\frac{(-1)^{n+1}(2n-1)!\ (2880n^6+5760n^5-4848n^4-10816n^3 -420n^2+2344n-405)}{2^{4n+4}(n+1)!(n+2)!(2n+1)^2 (2n+3)^2(2n+5)(12n^2-16n+1)}$	$2n+4$

TABLE 11
Ratio of error coefficients; staggered/regular grid.

	Accuracy order							
	$p=2$	4	6	8	10	12	14	16
Explicit	0.2500	0.1406	.0.0977	0.0748	0.0606	0.0509	0.0439	0.0386
3-diag.		0.5313	0.3574	0.2625	0.2065	0.1701	0.1445	0.1256
5-diag.			0.5734	0.4958	0.3915	0.3172	0.2656	0.2281
7-diag.				0.5914	0.5356	0.4831	0.4083	0.3483
9-diag.					0.6014	0.5575	0.5165	0.4766
11-diag.						0.6078	0.5715	0.5375
13-diag.							0.6122	0.5813
15-diag.								0.6155

After writing this in the form $[1\ 4\ 1]f' = [-3\ 0\ 3]f$ (to get ones at the edge of the f'-stencil), the LU factorization takes the form

$$\begin{bmatrix} \alpha_1 & & & & \\ 1 & \alpha_2 & & & \\ & 1 & \ddots & & \\ & & \ddots & \ddots & \\ & & & 1 & \alpha_s \end{bmatrix} \begin{bmatrix} 1 & \beta_1 & & & \\ & 1 & \beta_2 & & \\ & & \ddots & \ddots & \\ & & & \ddots & \beta_{s-1} \\ & & & & 1 \end{bmatrix} \begin{bmatrix} \\ \\ f' \\ \\ \\ \end{bmatrix}$$

$$= \begin{bmatrix} & 3 & & & \\ -3 & & 3 & & \\ & -3 & & \ddots & \\ & & \ddots & 3 & \\ & & & -3 & \end{bmatrix} \begin{bmatrix} \\ \\ f \\ \\ \\ \end{bmatrix}.$$

The cost for each entry becomes (with "$-$," "$\times$," and "/" denoting the type of operation)

for right-hand side (RHS)	$1-$, $1\times$,
for U back subst.	$1-$, $1\times$,
for L back. subst.	$1-$, $1/$.

By storing $1/\alpha_i$ instead of α_i, the divide also becomes a multiply. The total operation count becomes six in this case, made up of equally as many subtractions and multiplications. This case is seen in the 3-diagonal, $(n=1)$-entry in Table 9. The other entries in this table are obtained similarly.

7. Comparison of accuracies and cost-effectiveness. The leading error coefficient in a finite difference formula does not give a very good impression of the formula's accuracy or of its utility. In particular, for higher order methods, it may not dominate further terms. Also, it offers little help in comparing methods of different formal orders. Nevertheless, it may be of interest to note from Tables 10 and 11 that staggering is always beneficial. The advantage is seen to increase with order but decrease with the number of diagonals used.

A frequently used alternative error comparison approach (e.g., [5], [17]) consists of inspecting how the different derivative approximations treat a pure Fourier mode $e^{i\omega x}$ on a grid over, say, $[-1,1]$ with grid spacing h. The modes that can be represented

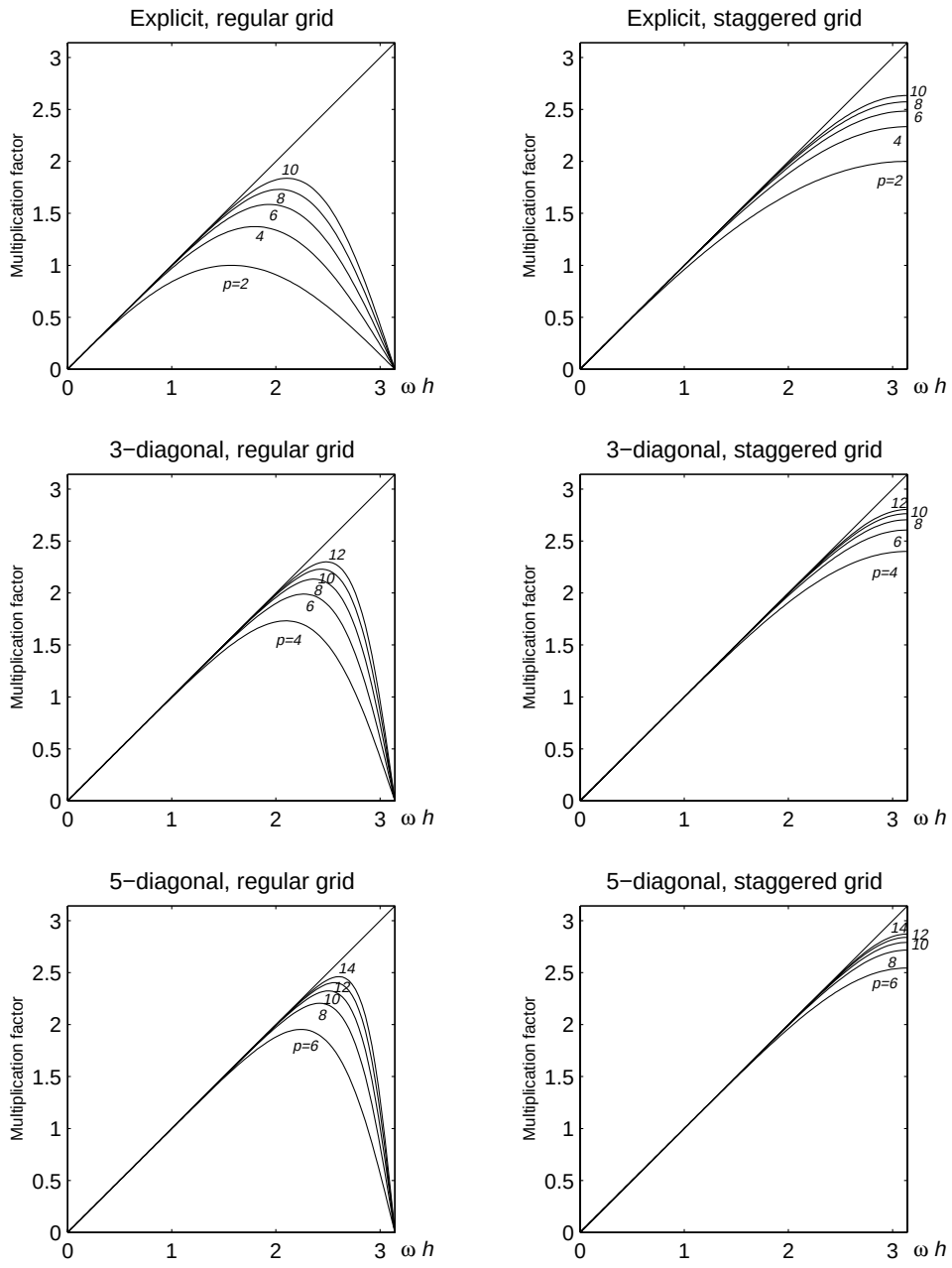

FIG. 6. *Fourier multiplication factors for different methods, displayed against ωh. The curves are labeled according to the order of accuracy p of the methods.*

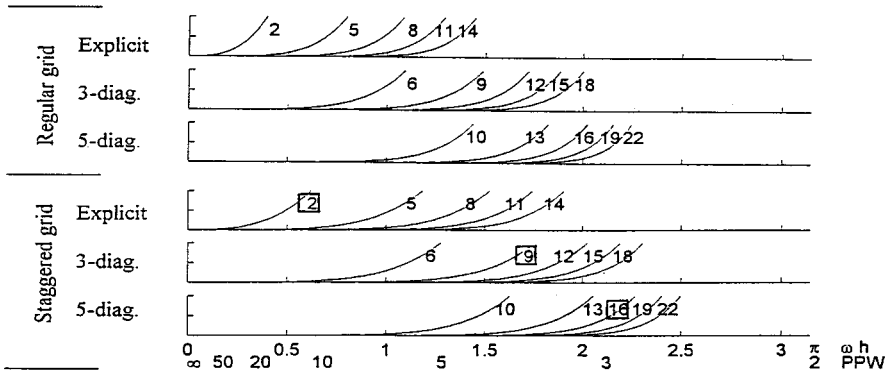

FIG. 7. *Deviation of the Fourier multiplication factors from the ideal straight line for all the cases shown in Figure* 5. *The horizontal axis is labeled in both frequency* ωh *and in points per wavelength (PPW). The vertical axis in each subplot extends to* 0.01. *All curves are labeled according to the operation count per grid point, as given in Table* 9. *The "boxed" numbers mark schemes that are particularly advantageous in their respective accuracy ranges.*

on the grid will satisfy $-\pi < \omega h < \pi$; higher modes will appear equivalent to a lower one on the grid by aliasing. The derivative of $e^{i\omega x}$ is

$$\frac{d}{dx}e^{i\omega x} = i\omega e^{i\omega x} = (\omega h)\frac{i}{h}e^{i\omega x},$$

whereas the explicit, regular grid, second order FD approximation would give

$$\left[\frac{1}{2}e^{i\omega(x+h)} - \frac{1}{2}e^{-i\omega(x-h)}\right]/h = (\sin\omega h)\frac{i}{h}e^{i\omega x}.$$

These factors (ωh and $\sin\omega h$) are seen as the diagonal straight line and the bottom curve, respectively, in the top left subplot of Figure 6. The $\sin(\omega h)$-curve is seen to be approximately correct only for a small fraction of the Fourier mode the grid can represent; using it is extremely wasteful on data storage (as well as on computational efficiency). As the order of accuracy p is increased, the coverage over $\omega h = [0, \pi]$ clearly improves.

The other five subplots in Figure 6 show how coverage is gained both by adding diagonals (i.e., turning to implicit approximations) and by using staggering. The fact that the curves for staggered approximations are not forced to zero at $\omega h = \pi$ (but instead have zero slope there) allows them to provide a better coverage across the spectrum.

A major advantage of this spectral comparison method (as opposed to looking at error coefficients) is that we can directly compare methods of different orders of accuracy. To better see the differences between the methods, we show in Figure 7 how the different curves in Figure 6 deviate from the exact results. In this figure, the curves are not labeled according to their accuracy but according to the computational cost per grid point, as displayed in Table 9. We note that for either type of grid, there is a significant improvement in going from explicit to 3-diagonal schemes, but to proceed further to 5-diagonal does not improve efficiency much (if at all). Staggering is again

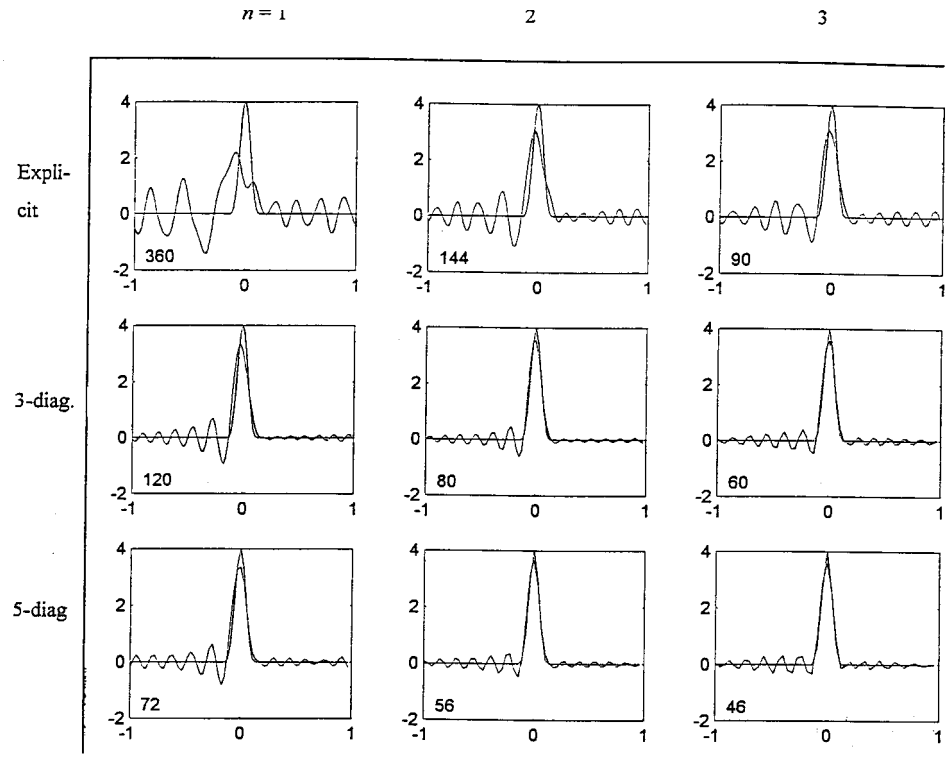

FIG. 8. *Regular grid solutions at $t = 100$ using different spatial approximations. The grid sizes (shown in the bottom-left corner of each subplot) were selected to make each case equally costly in computer time (assuming 1-D).*

seen as clearly advantageous in all cases. The three schemes that are highlighted as particularly effective in Figure 7 are all staggered, and they have the stencils

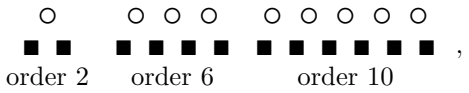

where "■" denotes a (known) function value entry and "○" denotes an (unknown) derivative value entry.

8. Test problem. As a simple test problem, we consider

$$u_t + u_x = 0; \quad \text{periodic over } [-1,1],$$
$$\text{initial condition } u(x,0) = \begin{cases} \left[1+\cos\left(\frac{\pi x}{0.15}\right)\right]^2 & |x| < 0.15, \\ 0 & |x| > 0.15. \end{cases}$$

This equation is discretized in space, and its solution advanced analytically in time (i.e., the displays in Figures 8–11 show only spatial errors). Figure 8 shows the

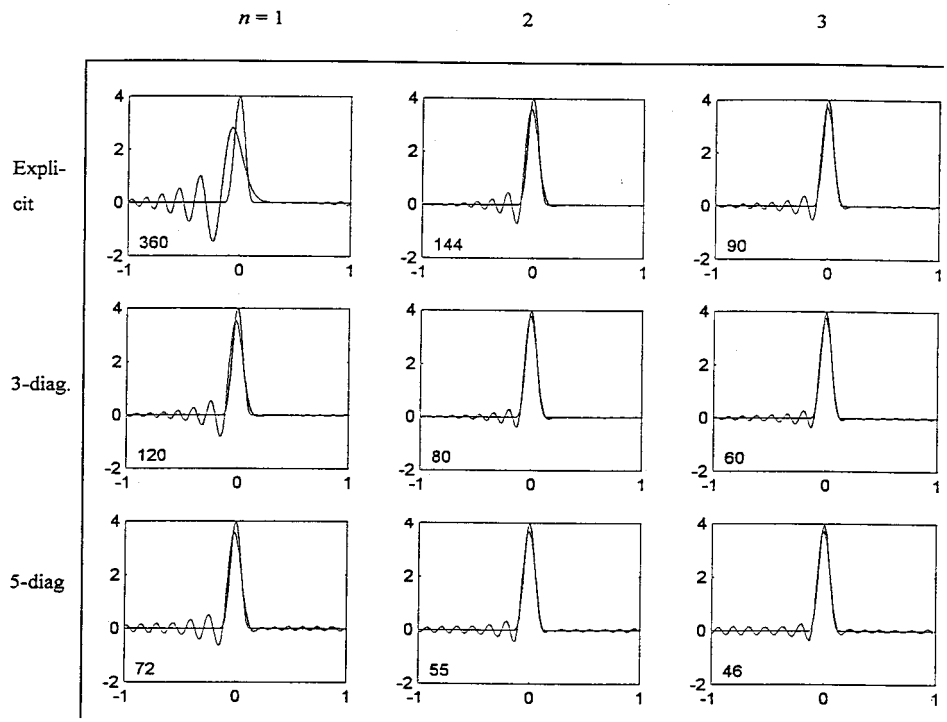

FIG. 9. *Same as Figure* 8, *but using staggered approximations for the spatial derivative. The reductions in the amplitudes of the dispersive wave trains* (*compared to the regular grid cases in Figure* 8) *are particularly noticeable if one compares the wave trains as they leave the left edge of the domains and, because of the periodicity, reappears in the right half of the subplots.*

numerical and exact solutions for a regular grid with different methods at time $t = 100$, i.e., after the pulse has traversed the period 50 times. The number shown in the bottom left of each subplot tells the number of spatial grid points used—this was selected so that, based on the operations count in Table 9, all cases would be equally costly if run in 1-D. Figure 9 shows the equivalent data for staggered grids. As expected from our analysis, staggering is advantageous in all the cases (but much less so for the most implicit scheme).

Higher dimensions (2-D and 3-D) and also longer time integration strongly favor higher order methods over lower order ones. Figure 10 shows the same test run to time $t = 2000$ using grid sizes (in each spatial direction) which provide equal cost in 2-D. In Figure 11, we refine the Explicit ($n = 1$)-scheme successively. The additional number within each subplot shows the relative computer time required (with "1" corresponding to the cost of each of the cases in Figure 10). It is clear that to achieve acceptable—say about 1%—accuracy requires exorbitant computational costs (scaling the same in both time and memory). The bottom-left subplot in Figure 11 shows comparable accuracy to the bottom-right one in Figure 9—at about a 4000 times larger cost (in 3-D, this factor increases to about 260,000). The staggered second order scheme in this comparison corresponds to the Yee scheme, which when first proposed in 1966 was pioneering for time-dependent computational electromagnetics

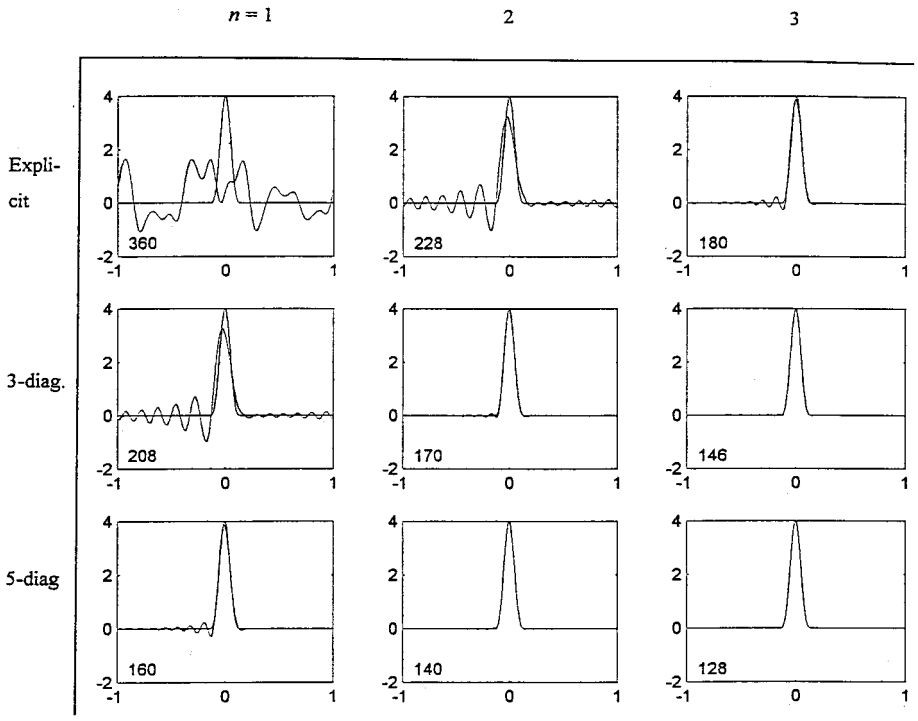

FIG. 10. *Solutions for staggered grid at* $t = 2000$ *with grid sizes selected to make computations equally time consuming in* 2*-D. (The memory requirements scale with the square of the numbers are given in the bottom left corners.)*

(Maxwell's equations) [22]. It has since enjoyed a long-lasting popularity (e.g., [16], [20]) in spite of its low order of accuracy.

9. Conclusions. Combining

- high orders of accuracy (i.e., wider stencils),
- implicitness, and
- staggering

leads to a class of computationally very cost-effective finite difference schemes. As their orders of accuracy are increasing, these schemes approach in accuracy the well-known spectral accuracy of periodic, explicit PS schemes. The schemes are defined on equispaced Cartesian grids. When combined with the idea of overlapping subdomains, the relatively narrow stencil widths make the schemes well-suited for computations in media with curvilinear material interfaces. The schemes can be applied to most wave-type PDEs of broad interest. In the particular application of time-domain computational electromagnetics (TDCEM), the classical Yee scheme satisfies only the last of the three conditions above—we find that major improvements in efficiency can be achieved by also accommodating the other two conditions.

This paper quotes a large number of results, often with few hints about their derivations. More details in that respect are found in [9].

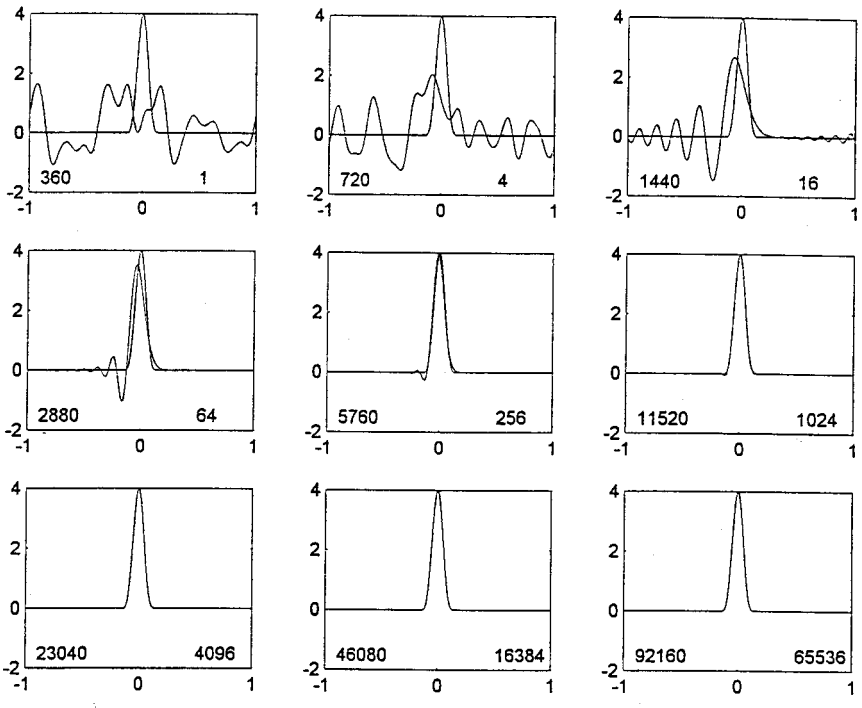

FIG. 11. *Solutions at* $t = 2000$ *for the staggered explicit* $n = 1$ *(Yee-type) scheme for increasingly fine grids. The numbers in the bottom-left corners denote—as before—the number of grid points across the period. The numbers in the bottom-right corners give the relative cost in both computer time and memory, if implemented in* 2*-D, compared to the unit* (1) *cost of all the cases in Figure* 10*. The top-left subplot of Figures* 10 *and* 11 *are identical—we see here how costly it is to achieve high accuracy by refining the grid in this scheme.*

REFERENCES

[1] Y. ADAM, *Highly accurate compact implicit methods and boundary conditions*, J. Comput. Phys., 24 (1977), pp. 10–22.

[2] L. COLLATZ, *The Numerical Treatment of Differential Equations*, Springer-Verlag, Berlin, 1960.

[3] T. A. DRISCOLL AND B. FORNBERG, *A block pseudospectral method for Maxwell's equations:* I. *One-dimensional, discontinuous-coefficients case*, J. Comput. Phys., 140 (1998), pp. 1–19.

[4] T. A. DRISCOLL AND B. FORNBERG, *Block pseudospectral methods for Maxwell's equations:* II. *Two-dimensional, discontinuous-coefficients case*, SIAM J. Sci. Comput., to appear.

[5] B. FORNBERG, *On a Fourier method for the integration of hyperbolic equations*, SIAM J. Numer. Anal., 12 (1975), pp. 509–528.

[6] B. FORNBERG, *High-order finite differences and the pseudospectral method on staggered grids*, SIAM J. Numer. Anal., 27 (1990), pp. 904–918.

[7] B. FORNBERG, *A Practical Guide to Pseudospectral Methods*, Cambridge University Press, Cambridge, UK, 1996.

[8] B. FORNBERG, *Calculation of weights in finite difference formulas*, SIAM Rev. 40 (1998), pp. 685–691.

[9] M. GHRIST, *Finite Difference Methods for Wave Equations*, Ph.D. thesis, Univ. of Colorado at Boulder, Boulder, CO, in preparation.

[10] M. GHRIST, T. A. DRISCOLL, AND B. FORNBERG, *Staggered time integrations for wave equations*, SIAM J. Sci. Comput., submitted.

[11] R. S. Hirsch, *Higher-order accurate difference solutions of fluid mechanics problems by a compact differencing technique*, J. Comput. Phys., 19 (1975), pp. 90–109.
[12] R. S. Hirsch, *High-Order Approximations in Fluid Mechanics*, VKI Lecture Series 1983-04, Von Karman Inst. for Fluid Dyn., Brussels, 1983.
[13] O. Holberg, *Computational aspects of the choice of operator and sampling interval for numerical differentiation in large-scale simulation of wave phenomena*, Geophys. Prospecting, 35 (1987), pp. 629–655.
[14] M. Kindelan, A. Kamel, and P. Sguazzero, *On the construction and efficiency of staggered numerical differentiators for the wave equation*, Geophysics, 55 (1990), pp. 107–110.
[15] Z. Kopal, *Numerical Analysis*, 2nd ed., Chapman and Hall, London, 1961.
[16] K. S. Kunz and R. J. Lubbers, *The Finite Difference Time Domain Method for Electromagnetics*, CRC Press, Boca Raton, FL, 1993.
[17] S. K. Lele, *Compact finite difference schemes with spectral-like resolution*, J. Comput. Phys., 103 (1992), pp. 16–42.
[18] R. Mittet, O. Holberg, B. Arntsen, and L. Amundsen, *Fast finite difference modeling of 3-D elastic wave equation*, Soc. Exploration Geophysics Expanded Abstracts, 1 (1988), pp. 1308–1311.
[19] S. A. Orszag and M. Israeli, *Numerical simulation of viscous incompressible flows*, Ann. Rev. Fluid Mech., 6 (1974), pp. 281–318.
[20] A. Taflove, *Computational Electrodynamics: The Finite-Difference Time-Domain Method*, Artech House, Boston, 1995.
[21] R. Vichnevetsky and J. B. Bowles, *Fourier Analysis of Numerical Approximations of Hyperbolic Equations*, Studies in Appl. Math. 5, SIAM, Philadelphia, PA, 1982.
[22] K. S. Yee, *Numerical solution of initial boundary value problems involving Maxwell's equations in isotropic media*, IEEE Trans. Antennas and Propagation, 14 (1966), pp. 302–307.